
**Liquid Crystals**
Publication details, including instructions for authors and subscription information:
http://www.informaworld.com/smpp/title~content=t713926090

# Anisotropy of domain growth in nematic liquid crystals

Jinkyung Jung[a]; Colin Denniston[b]; Enzo Orlandini[c]; Julia M. Yeomans Corresponding author[a]
[a] Dept. of Physics, Theoretical Physics, University of Oxford, Oxford OX1 3NP, UK [b] Dept. of Physics and Astronomy, The Johns Hopkins University, Baltimore, MD 21 218, USA [c] INFM-Dipartimento di Fisica, Universita di Padova, I-35131 Padova, Italy

Online publication date: 07 July 2010

**To cite this Article** Jung, Jinkyung , Denniston, Colin , Orlandini, Enzo and Yeomans Corresponding author, Julia M.(2003) 'Anisotropy of domain growth in nematic liquid crystals', Liquid Crystals, 30: 12, 1455 — 1462
**To link to this Article: DOI:** 10.1080/02678290310001622489
**URL:** http://dx.doi.org/10.1080/02678290310001622489

LIQUID CRYSTALS, VOL. 30, NO. 12, DECEMBER 2003, 1455–1462



# Anisotropy of domain growth in nematic liquid crystals

JINKYUNG JUNG, COLIN DENNISTON†, ENZO ORLANDINI‡ and JULIA M. YEOMANS*

Dept. of Physics, Theoretical Physics, University of Oxford, 1 Keble Road, Oxford OX1 3NP, UK

†Dept. of Physics and Astronomy, The Johns Hopkins University, Baltimore, MD 21 218, USA

‡INFM-Dipartimento di Fisica, Universita di Padova, I-35131 Padova, Italy

(*Received 19 December 2002; in final form 3 July 2003; accepted 17 July 2003*)

We have studied domain growth in nematic liquid crystals using a lattice Boltzmann algorithm to solve the full, three-dimensional equations of hydrodynamics. An initially cylindrical V (bend) domain in an H (splay) state grows or shrinks *anisotropically* in agreement with experiment. A $\pm\frac{1}{2}$ disclination loop forms at the mid-point of the wall surrounding the domain. We argue that different director configurations at different points on the loop lead to velocity anisotropy and show that both elastic effects and backflow are relevant. We discuss the dependence of the domain wall velocity on surface tilt and on the magnitude of an applied electric field.



## 1. Introduction

The dynamics of defects in liquid crystals can have a marked effect on their physical properties [1]. In particular, switching between topologically distinct configurations in a liquid crystal device can involve the nucleation and growth of a domain of the switched state. For example, Acosta *et al.* [2] have reported results showing how the speed at which a cylindrical V (bend) domain grows at the expense of an H (splay) domain in a pi-cell device depends on the surface tilt angle, applied field and cell thickness. They find, as expected, that many features of their results can be explained by assuming a rate of growth proportional to the free energy difference between the growing and shrinking phases.

However a particularly interesting, unexplained feature of the experiments is an anisotropy in the speed of the domain wall bounding the growing state. This leads to domains losing their circular symmetry as they grow. Acosta *et al.* [2] speculated that this was due to backflow effects.

The aim of this paper is to model the growth of a V domain into an H matrix to explain the reasons behind the anisotropic growth. We find that there are two contributions to the anisotropy. The first of these is a relaxational effect that depends on the elastic coefficients. The second is hydrodynamic in origin and results from the back flow induced as the wall moves. Both effects occur because, moving around the domain, the wall changes its nature: from splay–bend with a $+\frac{1}{2}$ defect at its mid-point; to twist; to splay–bend with a $-\frac{1}{2}$ defect at its mid-point; and back to twist. The different director configurations lead to differences in both the relaxational dynamics and the flow.

The results were obtained by using a lattice Boltzmann approach to solve the Beris–Edwards equations of liquid crystal hydrodynamics. These rather general equations are needed to describe liquid crystal hydrodynamics in regions where there is a variation in the magnitude of the order parameter; they are presented in §2. The geometry of the simulation is described in §3. To describe fully the disclination loop we work in three dimensions, extending the two-dimensional results described in [3]. Results are presented in §4 where we discuss the effects of surface tilt, elastic constants, back flow and an applied voltage on the domain growth.

*Author for correspondence; e-mail: j.yeomans1@physics.ox.ac.uk

## 2. Theory

To describe the movement of topological defects, in particular backflow effects, it is important to use a formulation of liquid crystal hydrodynamics that is written in terms of the tensor order parameter **Q**. This allows the magnitude of the order parameter to vary [4, 5] and correctly describes the dynamics of the defect cores.

The tensor order parameter is related to the direction

*Liquid Crystals* ISSN 0267-8292 print/ISSN 1366-5855 online © 2003 Taylor & Francis Ltd
http://www.tandf.co.uk/journals
DOI: 10.1080/0267829031000162248 9

of individual molecules $\hat{m}$ by

$$Q_{\alpha\beta} = <\hat{m}_\alpha \hat{m}_\beta - \frac{1}{3}\delta_{\alpha\beta}> \quad (1)$$

where the angular brackets denote a coarse-grained average. (Greek indices will be used to represent Cartesian components of vectors and tensors and the usual summation over repeated indices will be assumed.) $\mathbf{Q}$ is a traceless symmetric tensor. Its largest eigenvalue, $\frac{2}{3}q$, $0<q<1$, describes the magnitude of the order. The corresponding eigenvector $\mathbf{n}$ describes the director field. (The more widely used Ericksen–Leslie–Parodi formulation [6, 7] of the equations of motion for liquid crystals, written in terms of the director field $\mathbf{n}$, assumes that eigenvalues of $\mathbf{Q}$ are of constant magnitude.)

The equilibrium properties of the liquid crystal are modelled by a Landau–de Gennes free energy [8, 9]

$$F = \int_V \mathrm{d}V (f_{\text{bulk}} + f_{\text{elastic}} + f_{\text{electric}}). \quad (2)$$

$f_{\text{bulk}}$ describes the bulk free energy density [10]

$$f_{\text{bulk}} = \frac{A_0}{2}\left(1-\frac{\gamma}{3}\right) Q_{\alpha\beta}^2 - \frac{A_0\gamma}{3}\, Q_{\alpha\beta}Q_{\beta\gamma}Q_{\gamma\alpha} + \frac{A_0\gamma}{4}\left(Q_{\alpha\beta}^2\right)^2, \quad (3)$$

$f_{\text{elastic}}$ is the elastic free energy density

$$f_{\text{elastic}} = \frac{L_1}{2}\left(\partial_\alpha\, Q_{\beta\gamma}\right)^2 + \frac{L_2}{2}\left(\partial_\alpha\, Q_{\alpha\gamma}\right)\left(\partial_\beta\, Q_{\beta\gamma}\right) + \frac{L_3}{2} Q_{\alpha\beta}\left(\partial_\alpha\, Q_{\gamma\varepsilon}\right)\left(\partial_\beta\, Q_{\gamma\varepsilon}\right), \quad (4)$$

and the electric contribution is

$$f_{\text{electric}} = -\frac{\varepsilon_{\text{m}}}{8\pi}E^2 - \frac{\varepsilon_{\text{a}}}{12\pi}E_\alpha E_\beta Q_{\alpha\beta} \quad (5)$$

where

$$\varepsilon_{\text{a}} = \frac{3}{2q}\left(\varepsilon_\parallel - \varepsilon_\perp\right),\ \varepsilon_{\text{a}} = \frac{2}{3}\varepsilon_\perp + \frac{1}{3}\varepsilon_\parallel \quad (6)$$

and $\varepsilon_\parallel$ and $\varepsilon_\perp$ are the components of the dielectric constants parallel and perpendicular to the director field, respectively.

The Beris–Edwards equation of motion for the nematic order parameter is [11]

$$(\partial_{\text{t}} + \mathbf{u}\cdot\nabla)\,\mathbf{Q} - \mathbf{S}(\mathbf{W}, \mathbf{Q}) = \Gamma\mathbf{H} \quad (7)$$

where $\Gamma$ is a collective rotational diffusion constant. The first term on the left-hand side of equation (7) is the material derivative describing the usual time dependence of a quantity advected by a fluid with velocity $\mathbf{u}$. This is generalized by a second term

$$\mathbf{S}(\mathbf{W}, \mathbf{Q}) = (\xi\,\mathbf{W}_{\text{s}} + \mathbf{W}_{\text{a}})\left(\mathbf{Q} + \frac{1}{3}\mathbf{I}\right) + \left(\mathbf{Q} + \frac{1}{3}\mathbf{I}\right)(\xi\,\mathbf{W}_{\text{s}} - \mathbf{W}_{\text{a}}) - 2\xi\left(\mathbf{Q} + \frac{1}{3}\mathbf{I}\right)\mathrm{Tr}(\mathbf{QW}) \quad (8)$$

where $\mathbf{W}_{\text{s}} = (\mathbf{W} + \mathbf{W}^{\text{T}})/2$ and $\mathbf{W}_{\text{a}} = (\mathbf{W} - \mathbf{W}^{\text{T}})/2$ are the symmetric part and the anti-symmetric part, respectively, of the velocity gradient tensor $W_{\alpha\beta} = \partial_\beta u_\alpha$. $\mathbf{S}(\mathbf{W}, \mathbf{Q})$ appears in the equation of motion because the order parameter distribution can be both rotated and stretched by flow gradients. This is a consequence of the rod-like geometry of the liquid crystal molecules. $\xi$ is a constant which depends on the molecular details of a given liquid crystal. The term on the right-hand side of equation (7) describes the relaxation of the order parameter towards the minimum of the free energy. The molecular field $\mathbf{H}$ which provides the driving force is related to the variational derivative of the free energy by

$$\mathbf{H} = -\frac{\delta \mathrm{F}}{\delta \mathbf{Q}} + \frac{\mathbf{I}}{3}\,\mathrm{Tr}\,\frac{\delta \mathrm{F}}{\delta \mathbf{Q}}. \quad (9)$$

The fluid momentum obeys the continuity

$$\partial_{\text{t}}\rho + \partial_\alpha \rho u_\alpha = 0 \quad (10)$$

and the Navier–Stokes equation

$$\rho\left(\partial_{\text{t}} + u_\beta\partial_\beta\right)u_\alpha = \partial_\beta\tau_{\alpha\beta} + \partial_\beta\sigma_{\alpha\beta} + \eta\partial_\beta\left[\left(1-3\sigma_\rho P_0\right)\partial_\gamma u_\gamma \sigma_{\alpha\beta} + \partial_\alpha u_\beta + \partial_\beta u_\alpha\right] \quad (11)$$

where $\rho$ is the fluid density and $\eta$ is an isotropic viscosity (due to the structure of the stress tensor described below there are still five non-zero Leslie coefficients, although they are not all independent [11]). The form of this equation is not dissimilar to that for a simple fluid. However the details of the stress tensor reflect the additional complications of liquid crystal hydrodynamics. There is a symmetric contribution

$$\sigma_{\alpha\beta} = -P_0\delta_{\alpha\beta} - \xi H_{\alpha\gamma}\left(Q_{\gamma\beta} + \frac{1}{3}\delta_{\gamma\beta}\right) - \xi\left(Q_{\alpha\gamma} + \frac{1}{3}\delta_{\alpha\gamma}\right)H_{\gamma\beta} + 2\xi\left(Q_{\alpha\beta} + \frac{1}{3}\delta_{\alpha\beta}\right)Q_{\gamma\varepsilon}H_{\gamma\varepsilon} - \partial_\beta Q_{\gamma\nu}\frac{\delta F}{\delta\partial_\alpha Q_{\gamma\nu}} \quad (12)$$

and an antisymmetric contribution

$$\tau_{\alpha\beta} = Q_{\alpha\gamma}H_{\gamma\beta} - H_{\alpha\gamma}Q_{\gamma\beta}. \quad (13)$$

The differential equations for the order parameter field and the flow field are coupled. The velocity field and its derivatives appear in the equation of motion for the order parameter, equation (7). Unless the flow field $\mathbf{u} = 0$ the dynamics given by equation (7) are not purely relaxational, and hydrodynamics can play an important role. Conversely, the order parameter field affects the dynamics of the flow field through the stress tensors, equations (12) and (13), which appear in the Navier–Stokes equation (11) and depend on $\mathbf{Q}$ and $\mathbf{H}$. This back-action of the order parameter field on the flow field is usually referred to as back flow.

To summarize, the dynamics of the liquid crystal is described by the solution of equations (7), (10) and (11). We solve these equations numerically using a

lattice Boltzmann algorithm; details of the algorithm are given in [12].

## 3. Simulation details

We consider a nematic liquid crystal confined between parallel plates at $z=0$, $z=L_z$ as shown in figure 1. The directors at the plates are constrained to lie in the $(y, z)$ plane at fixed angles $+\theta_t$, $-\theta_t$ to the plate at $z=0$, $z=L_z$ respectively. Initially we choose the director field to be aligned vertically within a cylindrical domain lying at the centre of the sample and horizontally, along $y$, outside. Within a few simulation steps a $\pm\frac{1}{2}$ disclination loop (shown as a thick line in figure 1) is created at the interface because the two domains are topologically distinct. Symmetry constrains the defect ring to lie at $z=L_z/2$. The defect ring then grows or shrinks (depending on the simulation conditions, e.g. the tilt angle of the surface or the electric field) to reach an equilibrium state which minimizes the free energy.

Figure 1 also shows cross-sections of the director field. Because the surface is rubbed in the $y$ direction (i.e. the surface directors lie along the $y$ axis) a cross-section perpendicular to the $x$ axis contains splay–bend domain walls. These are labelled SB1 and SB2 in figure 1. The defect at the mid-point of the wall has topological charge $+\frac{1}{2}$ and $-\frac{1}{2}$ at SB1 and SB2 respectively. The cross-section perpendicular to the $y$ axis, on the other hand, includes twist walls labelled T1 and T2. The nature of the walls varies continuously between these limits.

Our aim here is to measure the velocity of the domain wall as it moves towards equilibrium, and in particular to ascertain whether different points in the wall have different velocities. Therefore we need to identify numerically the position of the domain wall, or equivalently that of the disclination ring at its mid-point, as a function of time. In a real liquid crystal device different domains can be distinguished by exploiting the optical properties of the liquid crystal. In a simulation one way of distinguishing the two domains is by plotting the order parameter or the free energy density. For example, in figure 2 the largest eigenvalue of the tensor order parameter $\mathbf{Q}$ (which corresponds to the order parameter of the nematic liquid crystal assuming uniaxiality) is plotted over the $(x, y)$ plane which contains the defect ring $z=L_z/2$. The difference in its magnitude between the two domains (a) and (b) is not large. But at the defect ring it has a much smaller value.

In the simulations it proved most convenient to pinpoint the exact position of the defect ring by calculating the quantity [13]

$$D_{ijkl}=\frac{1}{2}\{1-\mathrm{sgn}[(\mathbf{n}_i\cdot\mathbf{n}_j)(\mathbf{n}_j\cdot\mathbf{n}_k)(\mathbf{n}_k\cdot\mathbf{n}_l)(\mathbf{n}_l\cdot\mathbf{n}_i)]\}. \quad (14)$$

If $D_{ijkl}=1$, a disclination line pierces the lattice square with directors $\mathbf{n}_i$, $\mathbf{n}_j$, $\mathbf{n}_k$, and $\mathbf{n}_l$ at its corners.

Unless otherwise stated simulation parameters were $A_0=1.0$, $L_1=0.04396$, $L_2=0.04447$, $L_3=0.06064$, $\Gamma=0.625$, $\xi=0.59$, $\rho=2.0$, $P_0=1.0$, $\gamma=3$, $q=0.5$, $\varepsilon_a=41.4$ and $\varepsilon_m=9.8$. Simulation and physical parameters were related as usual by choosing a length scale $L_0$ a time scale $T_0$ and a pressure scale $P_0$. A simulation

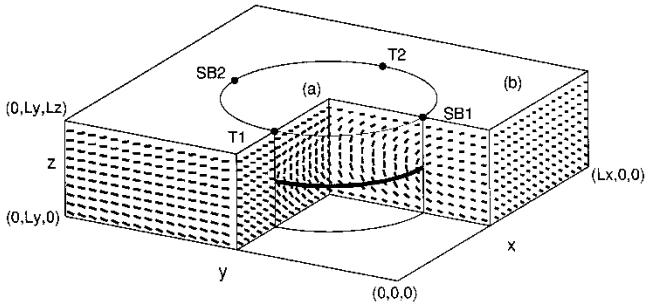


Figure 1. Schematic representation of the geometry used in the simulations. The inner cylindrical domain (a) has a V (bend) configuration and the outer domain (b) has an H (splay) configuration. At the middle of the domain wall ($z=L_z/2$), an $s=\pm\frac{1}{2}$ disclination loop is created (thick line), given a boundary condition of symmetrically tilted directors. T1, T2 are the points on the twist wall and SB1, SB2 lie on the splay–bend wall.

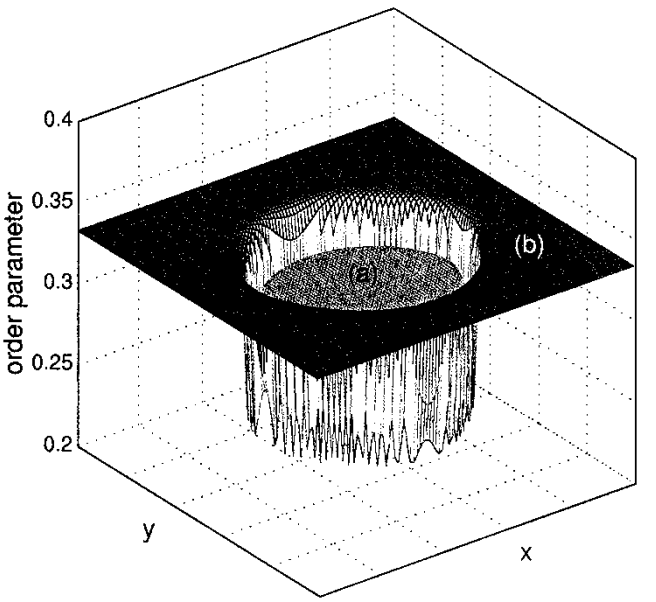


Figure 2. The largest eigenvalue of the tensor order parameter $\mathbf{Q}$ is plotted over the $(x, y)$ plane ($z=L_z/2$) which contains the defect ring. At the defect ring the eigenvalue has a much smaller value than in either of the two domains (a) or (b).

parameter with dimensions $[L]^{n_1}[T]^{n_2}[P]^{n_3}$, is multiplied by $L_0^{n_1}T_0^{n_2}P_0^{n_3}$ to give the physical value. $L_0 = 6.25\times10^{-8}$ m, $T_0 = 10^{-6}$ s and $P_0 = 10^5$ N m$^{-2}$ were chosen to give atmospheric pressure, elastic constants similar to those found for the common cyanobiphenyls such as 5CB or their mixtures such as E7, and physically realistic viscosities.

The mapping gives values for the Frank elastic constants of $K_{\text{splay}} = 11.0$ pN, $K_{\text{twist}} = 6.63$ pN, $K_{\text{bend}} = 16.9$ pN [9]. The lattice size was $L_x = 150$, $L_y = 150$ and $L_z = 10$. This corresponds to a cell of thickness $\sim 0.6\,\mu$m and lateral dimensions $\sim 10\,\mu$m. This thickness is similar to that used in the experiments, but the experimental domains had radii $\sim$mm. These lengths are not accessible with current computers and we were therefore only able to model domain growth at an earlier stage when the domain is smaller. The velocity (which showed a weak dependence on the radius of the cylindrical domain for radii $\lesssim 10$ lattice sites) was measured when the radius was 70 lattice sites.

## 4. Results

Figure 3 shows how the size and shape of the disclination loop change as a function of time. In these simulations, there was no external field and the surface tilts were (*a*) 20° and (*b*) 40°. The initial circular shape of the domain is lost showing that the speed differs at different points around the disclination loop.

When the surface tilt angle is 20°, figure 3 (*a*), the disclination ring shrinks at each point as time passes because the surface tilt favours an H domain. But when the angle is 40°, figure 3 (*b*), the speed of movement is slower and the point SB1 moves to the outside of the original circle, showing that the domain expands in this direction. This effect is discussed in more detail below.

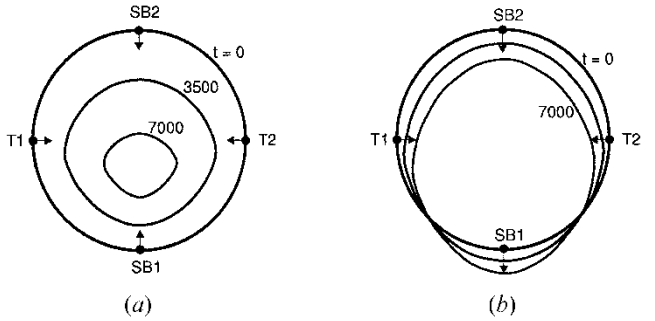


Figure 3. Change in the size and shape of a defect loop as a function of time for no external field and surface tilts (*a*) 20° and (*b*) 40°. The initial circular shape of the loop is lost because the speed differs at different points around the disclination loop.

### 4.1. *Backflow*

First, in order to isolate the effect of backflow without the complication of distortion, we restrict ourselves to one elastic constant $L_1 = 0.1$, $L_2 = L_3 = 0$. (This corresponds to the three Frank elastic constants being equal, $K_{\text{splay}} = K_{\text{twist}} = K_{\text{bend}} = 19.6$ pN.) The other simulation parameters are those given in § 3. Figure 4 (*a*) displays results with no backflow (i.e. we solve equation (7) with the constraint $\mathbf{u} = 0$). As expected, the wall velocity decreases with increasing surface tilt as the free energy advantage of the splay configuration is reduced. When the tilt angle is 45° the splay and bend configurations have equal free energies so the speed of the disclination loop approaches zero. (The line tension associated with the loop will tend to shrink it, but this is a small effect for a loop of this size.)

Without backflow, all points on the disclination loop have exactly the same speed at each surface tilt so a domain that is initially circular will maintain its shape. However when backflow is included the different points on the domain boundary move with different speeds, as shown in figure 4 (*b*). All the defects are accelerated, the $+1/2$ defect at SB1 most, the $-1/2$ defect at SB2 only slightly. This agrees with results obtained in two dimensions [3]. The two twist defects (T1, T2) still have exactly the same speed.

The effect of backflow in the vicinity of the defects can be explained by considering the velocity fields shown in figures 5 and 6. These are for the splay–bend walls (a cross-section through SB1 and SB2), and the twist walls (a cross-section through T1 and T2), respectively.

In figure 5 (*a*) the defect point on the left hand side has topological strength of $+\frac{1}{2}$ and corresponds to SB1 in figure 1. The velocity vortices in figure 5 (*b*) corresponding to this point are considerably stronger than those formed around the $-\frac{1}{2}$ defect (SB2) and hence are more efficient in increasing its velocity. In figure 6, at the two twist defects, the velocity vortices have the same magnitude and opposite directions so the influence of flow on speed is exactly the same for the two points.

### 4.2. *Elastic constants*

We now return to consider elastic constants appropriate to the liquid crystal E7. In figure 7 we plot the speed at points SB1, SB2, T1 and T2 on the disclination loop as a function of the surface tilt both with and without backflow. Again the speed of movement decreases as expected as the surface tilt increases because the free energy density difference between the H and V states decreases. Note, however, that even without backflow, points at different positions on the

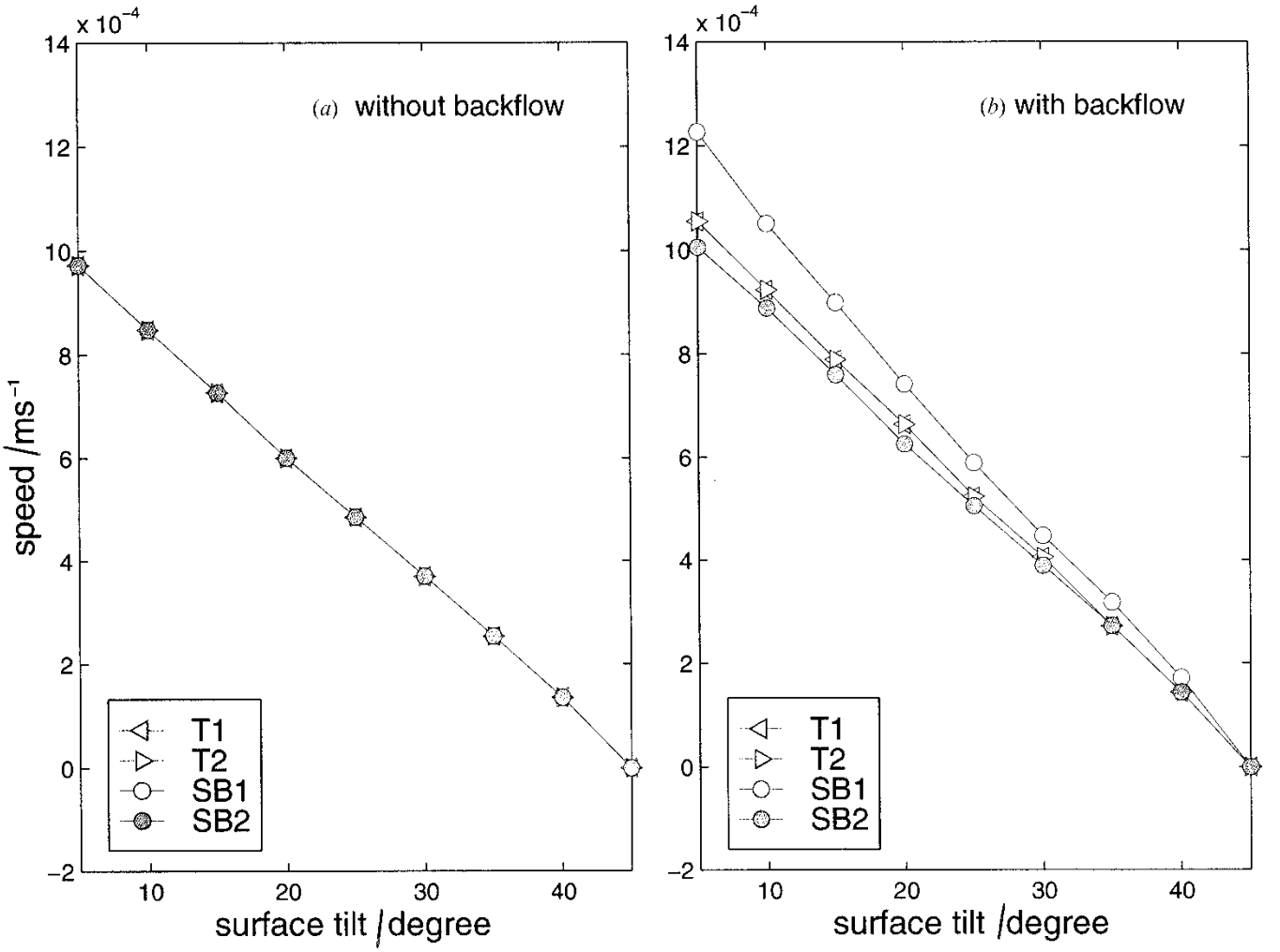


Figure 4. Velocity of four points (see notation of figure 1) on the disclination loop as a function of surface tilt (*a*) without backflow and (*b*) with backflow. The results are for $L_1=0.1$, $L_2=L_3=0$ corresponding to three equal Frank elastic constants.

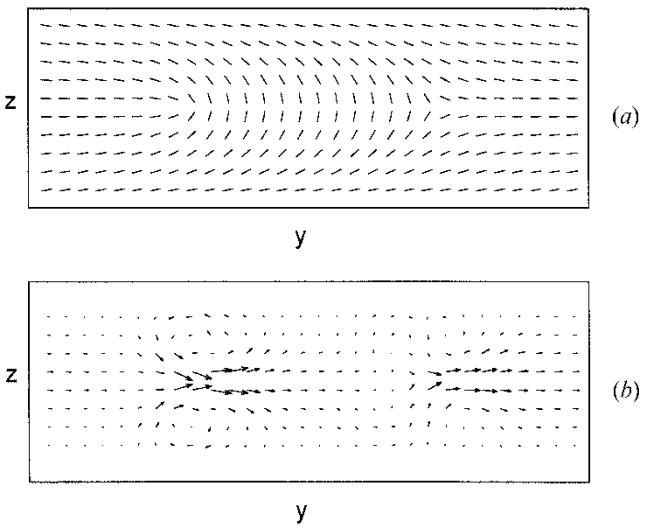


Figure 5. Cross sections of (*a*) the director field and (*b*) the velocity field for the splay–bend walls ($x=L_x/2$).

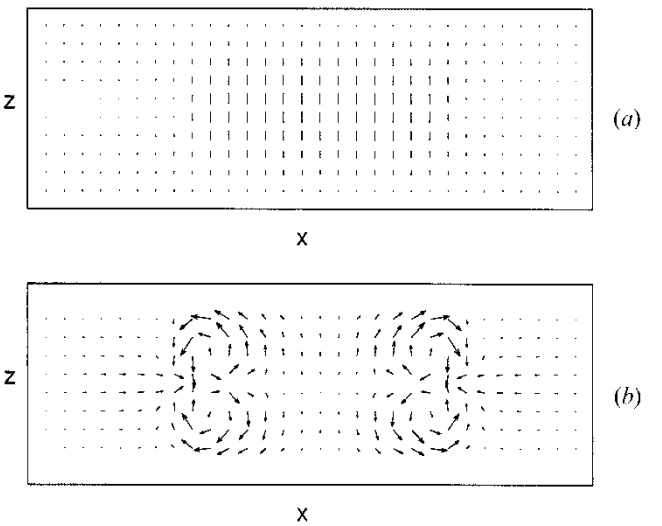


Figure 6. Cross sections of (*a*) the director field and (*b*) the velocity field for the twist walls ($y=L_y/2$).

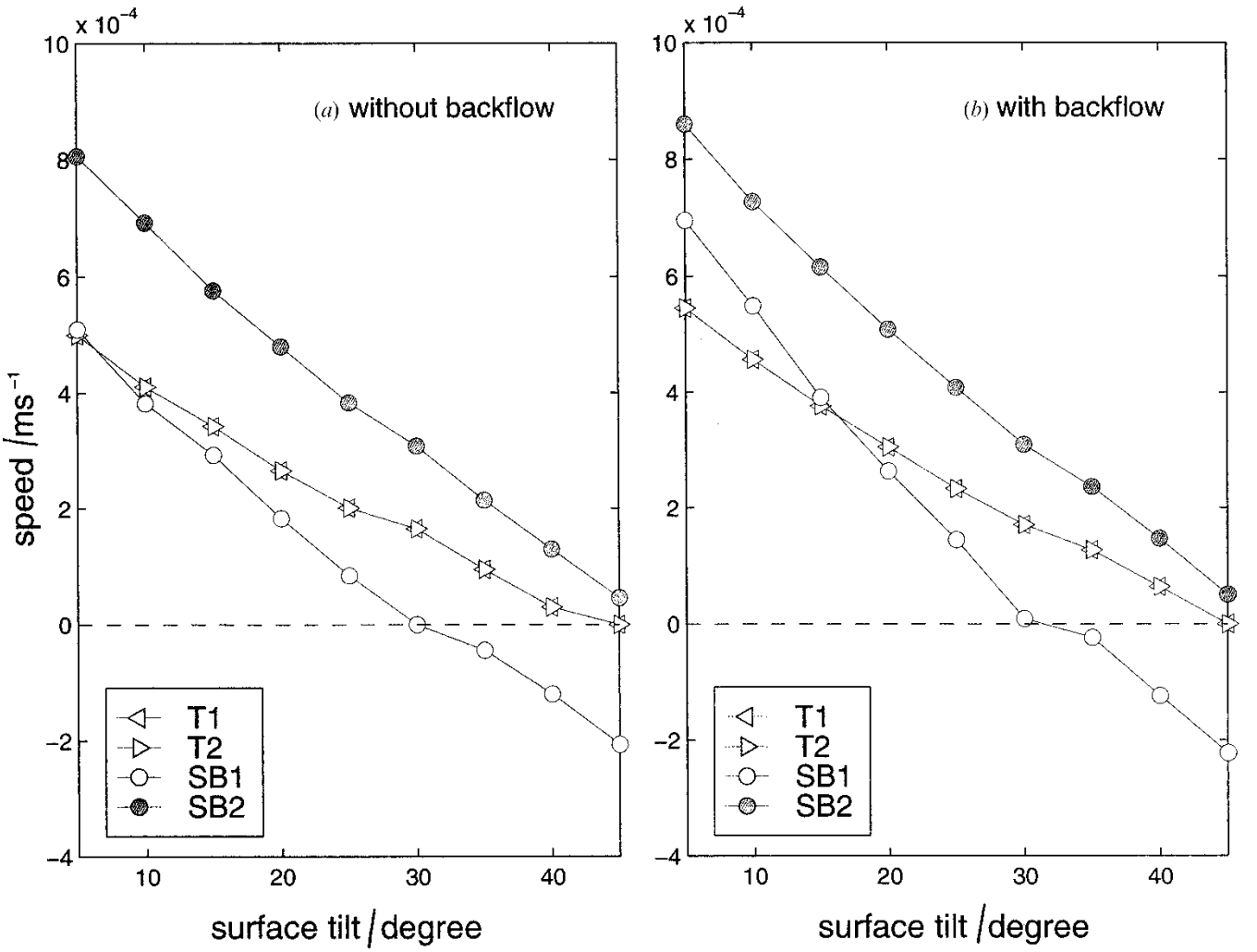


Figure 7. Velocity of four points (see notation of figure 1) on the disclination loop as a function of surface tilt (*a*) without backflow and (*b*) with backflow. Simulation parameters correspond to E7.



disclination ring have different speeds. Indeed, for these elastic constants, the velocity anisotropy depends more strongly on elastic effects than on back flow.

It is interesting to note that for the $+\frac{1}{2}$ defect (SB1) point, the direction of movement changes when the tilt angle is 30°. Hence the motion of the domain acquires a translational component as shown in figure 3 (*b*).

### 4.3. *Electric field*

Liquid crystal devices are operated by switching to a state with the desired optical properties on applying an electric field. As the electric field is applied, the free energy density of each state alters so that the equilibrium between the two domains is changed. When the surface tilt is less than a critical angle (which varies with the elastic constants) and there is no external field, a splay director configuration is more stable than a bend configuration. On applying a field, directors prefer to align with the field so that the bend configuration can become more stable than the splay configuration. Thus we expect that the rate of growth (or contraction) of the disclination loop will depend on the value of an applied field.

To investigate this effect we set the surface tilt to an angle of 11.5° and plot in figure 8 the velocity of points SB1, SB2, T1 and T2 as a function of the voltage across the liquid crystal. The contraction of the disclination loop driven by the surface tilt slows as the field is increased and for $V \sim 1\,\mathrm{V}$ the effect of the field dominates and the central bend domain expands. When the applied voltage is less than 1 V, the domain contracts fastest at SB2 $\left(-\frac{1}{2}\right)$. However when voltage is greater than 1 V, it expands fastest at SB1 $\left(+\frac{1}{2}\right)$. Except near the transition voltage ($\sim 1\,\mathrm{V}$),

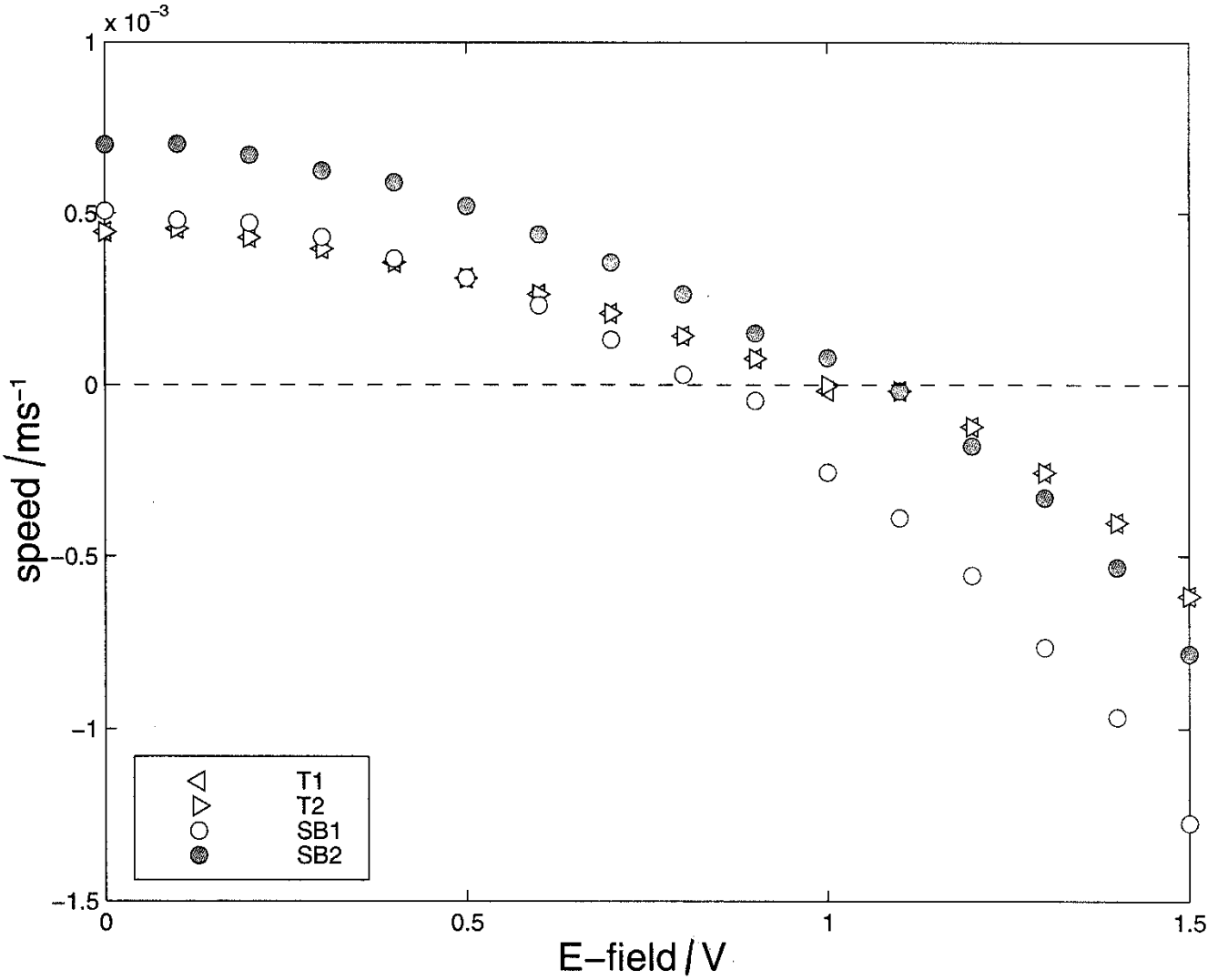


Figure 8. Velocity of four points (see notation of figure 1) on the disclination loop as a function of an applied voltage. Simulation parameters correspond to E7.

the two twist walls and remaining splay–bend wall move with similar speeds, as found in experiments [2].

Our simulations show higher speeds by a factor $\sim 10$ than the experiments. This is expected because of the different dimensions of the computational and experimental domains. In particular the disclination speed increases as the sample thickness decreases. For example, the speed of movement when the simulation width $L_z = 20$ is $\sim 30\%$ of that for $L_z = 10$.

## 5. Conclusions

This paper has presented a study of domain growth in nematic liquid crystals. The hydrodynamic equations were solved by using a lattice Boltzmann algorithm. Because we aimed to investigate the dynamics of a $s = \pm \frac{1}{2}$ disclination loop created on the domain wall, we chose to use the Beris–Edwards equations of motion for a tensor order parameter which allow for variations in the magnitude of the order parameter.

We found that an initially cylindrical V domain in an H state grows (or shrinks) anisotropically in agreement with experiment. We argued that this occurs because a preferred rubbing direction on the plates leads to different director configurations at different points on the boundary of the domain. Within the single elastic constant approximation, the anisotropy is solely due to backflow. However, for different elastic constants, relaxational dynamics also contributes and the domain grows anisotropically even if backflow is not taken into account. Indeed, for E7, this is the dominant effect.

Results were also presented showing that surface tilt and an applied electric field affect the speed at which the domain changes size because they affect the relative free energies of the H and V states.

Further work will be aimed at investigating the behaviour of defect loops in nematic liquid crystals whose motion is not driven by boundaries. It will also be of interest to compare simulation results with recent experiments on the dynamics of parallel disclination lines [14].

We thank E. J. Acosta, S. Elston, N. Mottram and G. Toth for helpful discussions. This work was supported by the Agency for Defence Development in Korea and the National Science Foundation under Grant No. 0 083 286.

## References

[1] Chung, I., Yurke, B., Pargellis, A. N., and Turok, N., 1993, *Phys. Rev. E*, **47,** 3343; Priezjev, N. V. and Pelcovits, R. A. 2002, *Phys. Rev. E*, **66,** 051705-1; Sonnet, A. M. and Virga, E. G. 1997, *Phys. Rev. E*, **56,** 6834; Wang, W. Shiwaku, T. and Hashimoto, T. 1998, *J. chem. Phys.*, **108,** 1618.

[2] Acosta, E. J., Towler, M. J., and Walton, H. G., 2000, *Liq. Cryst.*, **27,** 977.

[3] Toth, G., Denniston, C., and Yeomans, J. M., 2003, *Phys. Rev. E*, **67,** 051705.

[4] Schopohl, N., and Sluckin, T. J., 1987, *Phys. Rev. Lett.*, **59,** 2582.

[5] Sonnet, A., Kilian, A., and Hess, S., 1995, *Phys. Rev. E*, **52,** 718.

[6] Ericksen, J. L., 1966, *Phys. Fluids*, **9,** 1205.

[7] Leslie, F. H., 1968, *Arch. Ration. Math. Anal.*, **28,** 265.

[8] De Gennes, P. G., and Prost, J., 1993, *The Physics of Liquid Crystals*, 2nd Ed. (Oxford: Clarendon Press).

[9] Doi, M., and Edwards, S., 1989, *The Theory of Polymer Dynamics* (Oxford: Clarendon Press).

[10] Olmsted, P. D., and Lu, C.-Y. D., 1999, *Phys. Rev. E*, **60,** 4397.

[11] Beris, A. N., and Edwards, B. J., 1994, *Thermodynamics of Flowing Systems* (Oxford: Oxford University Press).

[12] Denniston, C., Orlandini, E., and Yeomans, J. M., 2001, *Phys. Rev. E*, **63,** 056702–1.

[13] Priezjev, N. V., and Pelcovits, R. A., 2001, *Phys. Rev. E*, **64,** 031710-1.

[14] Bogi, A., Martinot-Lagarde, P., Dozov, I., and Nobili, M. *Phys. Rev. Lett.*, **89,** 225501-1.